*Author's accepted manuscript: Journal of Nuclear Materials 458 (2015) 11–21*

# Interaction of He and He-V clusters with self-interstitials and dislocation defects in bcc Fe

D. TERENTYEV[1,*], N. ANENTO[2], A. SERRA[2] C.J. ORTIZ[3], E.E. ZHURKIN[4]

*[1]SCK•CEN, Nuclear Material Science Institute, Boeretang 200, B-2400 Mol, Belgium*
*[2]Department Matemàtica Aplicada III, E.T.S. Enginyeria de Camins, Universitat Politècnica de Catalunya, Jordi Girona 1-3, 08034 Barcelona, Spain*
*[3]Lab. Nacional de Fusión por Confinamiento Magnético, CIEMAT, 28040 Madrid, Spain*
*[4]Department of Experimental Nuclear Physics K-89, Institute of Physics, nanotechnology and telecommunications, St.Petersburg State Polytechnical University, 29 Polytekhnicheskaya str., 195251, St.Petersburg, Russia*

Abstract

The understanding of helium effects in synergy with radiation damage is crucial for the development of structural steels for fusion applications. Recent investigations in ultra-pure iron, taken as a basic model, have shown a drastic impact of dual beam (He-Fe) exposure on the accumulation of radiation-induced dislocation loops in terms of strong bias towards $a_0/2<111>$ family, while $a_0<100>$ loops are mostly observed upon Fe ion beam. In this work we perform a series of atomistic studies to rationalize possible mechanisms through which He could affect the evolution of microstructure and bias the population of $a_0/2<111>$ loops. Strong suppression of $a_0/2<111>$ loop migration, prohibiting their mutual interaction resulting in the formation of $a_0<111>$ and disappearance at sinks, is proposed to be caused by the He decoration occurring via helium-loop drag mechanism. A scenario for the microstructural evolution in the single- and dual-beam conditions is discussed.

*PACS: 71.15.Mb, 61.82.Bg; 61.80.Az; 61.72.Qq;*

Keywords: Helium, Iron, Dislocation Loop

*Corresponding author. Email: dterenty@sckcen.be; Tel.: +32-14-333197; fax: +32-14-321216.

1. Introduction

He embrittlement is one of the key issues to be addressed in the development and characterization of structural materials for fusion applications [1]. It is long known that He affects the evolution of microstructure in metals (see e.g. [2; 3]) and steels (see e.g. [4; 5; 6; 7]). One of the strongest effects of He upon irradiation at elevated temperature (i.e. 300°C and above) is the promotion of void swelling even in BCC Fe-Cr alloys which are superior with respect to swelling resistance [4; 8]. Another effect is the enhancement of the dislocation loop formation and preferential growth of cavities on dislocations [6; 9]. The effect of He on dislocation loop pattern may also have important consequences in a view of low-temperature embrittlement and high-temperature creep. Hence, an adequate knowledge of how He affects microstructural evolution not only in terms of voids but also dislocation loop population is an important unknown to be addressed in the current fusion R&D programme.

The presence of He upon irradiation (both electron and neutron) essentially influences the kinetics of the evolution of vacancy- and self-interstitial atom (SIA) type defects [9]. However, the full atomic-scale details on the interaction of He with point defects cannot be assessed by experiments. The interpretation of the experimental observations therefore requires certain assumptions about thermal stability, mobility and mutual interactions. The problem is especially evident if it comes to the interaction of He with point defect clusters, which, on the one hand, are not accessible to direct experimental observations, and on the other, have too large size to be considered by heavily demanding but rigorous *ab initio* calculations. Large scale molecular dynamics (MD) simulations are possible, however, the reliability of results is essentially determined by the quality of interatomic potentials, which keeps improving as more and more *ab initio* data appear.

On the *ab initio* side, the interaction of vacancies with interstitial He (occupying a tetrahedral position in bcc Fe) is relatively well studied by density functional theory (DFT). Several independent DFT works [10; 11; 12] in general converge to the following results:

(i) an interstitial He (henceforth $He_T$ since it occupies tetrahedral position) is deeply trapped by a single vacancy with binding energy $E_b$(He-V)=2.3 eV;

(ii) there is an optimum He-to-vacancy ratio offering a maximum thermal stability of $He_n$-$V_m$ clusters, which is n/m~1.3 corresponding to the dissociation energy of ~2.6 eV;

(iii) He-$V_2$ cluster has a migration energy of ~1.1 eV, which is lower than its dissociation energy (1.45 eV) and therefore should be considered as potentially mobile object at sufficiently high temperature (above ~ 450K).

The interaction of SIA defects with $He_T$ is less clear. A limited number DFT studies report that in BCC Fe, $He_T$ exhibits weak attraction to a <110> split dumbbell depending on its local position, with binding energies of 0.07 eV and 0.26 eV, respectively, reported in [12] and [13]. The interaction of a substitutional He with an SIA results in the recombination-replacement reaction releasing $He_T$ [13].

So far the interaction of $He_T$ with SIA clusters, small dislocation loops and straight dislocation lines was characterized only by the use of interatomic potentials. The most intensively exploited set of potentials was Fe-Fe developed by Ackland et al. in 1997 [14] and Fe-He developed by Wilson & Johnson [15; 16; 17]. There is a number of essential drawbacks of this set of potentials with regard to the properties of point- and extended lattice defects in bulk Fe [18] as well as He-defect interactions, concluded from the comparison with the above mentioned DFT data [12; 19]. The main drawbacks are the following:

(i) underestimated difference in the formation energy of a <110> split dumbbell and <111> crowdion;

(ii) incorrect ground state for small self-interstitial clusters (wrong migration mechanism and energy as a consequence);

(iii) three-fold degenerate structure for $a_0/2$<111> screw dislocation (here $a_0$ is the lattice unit, 0.286nm in bcc Fe);

(iii) incorrect ground state (octahedral instead of tetrahedral) for an interstitial He;

(iv) essentially overestimated He-vacancy binding energy;

(v) essentially overestimated or wrongly predicted sign of He-SIA interaction.

Although the information obtained with that potential (especially for He-SIA interaction) should be taken with precaution, below we summarized the results since it was extensively used to study He-dislocation and He-SIA interaction.

It was found that fast 1D migration of small <111> SIA clusters is not affected by the substitutional He (in concentration up to 2500 appm) [12]. The interaction of <111> SIA cluster (containing 11 SIAs) with a $He_4$-$V_6$ cluster results in the SIA-vacancy recombination and decoration of the remaining SIA cluster by He atoms. The decorated cluster was then seen to be immobile for the whole MD run (for 100 ps at 1000K). Given the significantly overestimated He-SIA interaction energy the latter result cannot be considered as a reliable one. From molecular static (MS) simulations [12], the binding energy between $He_T$ and <111> SIA cluster containing 20 defects is predicted to be 1.4 eV (and it goes up to 4.4 eV if four He atoms decorate the cluster). The binding of 1.4 eV is consistent with the estimation of the interaction energy of $He_T$ with $a_0/2$<111>{110} edge and screw dislocations, computed

using the same potential, being 1 eV and 2 eV, respectively [20; 21].. In addition, the latter works reported that interstitial He migrates along the dislocation line with an energy barrier of 0.4-0.5 eV for both screw and edge dislocations respectively.

Recently, several new interatomic potentials for Fe-He have been proposed to account for different properties obtained from DFT calculations [19; 22; 23; 24; 25]. Further studies with the updated potentials, involving $He_n$-$V_m$ clusters interacting with the edge dislocation, have shown that He-rich clusters are attracted to the tensile dislocation region, while vacancy-rich clusters are attracted to both dislocation sides [26]. Wang et al.[27] reported that a thermally stable $He_3$ cluster exhibits 1D migration in the core of the edge dislocation, in fact, the cluster moves faster on the dislocation line than in bulk. This result raises a question about the possibility of 1D-pipe diffusion not only on the straight dislocation but also on the dislocation loop.

From the experimental side, a number of fundamental studies in ultra-pure Fe and Fe-Cr alloys have been recently established to reveal mechanisms through which He influences the evolution of microstructure [28; 29; 30]. The most recent and statistically significant experimental observations reported by Prokhodtseva et al.[28] undoubtedly show that He atoms impacts the evolution of dislocation loop population, not only at 300°C and above, but at much lower temperatures as well. In particular, upon 500 keV $Fe^+$ and 10 keV $He^+$ irradiation at room temperature, 99% of loops have Burgers vector $a_0/2<111>$, while in a single Fe+ beam 89% of loops are of $a_0<100>$ type. The density of <100> loops was lower and the size was larger than that of $a_0/2<111>$ ones. The author's interpretation is that He suppresses the mobility of $a_0/2<111>$ loops, which otherwise escape to free surface or mutually interact producing $a_0<100>$ loops. Such reaction mechanism was already observed *in situ* in ultra pure Fe but upon 1 MeV $e^-$ irradiation (i.e. no cascades are produced) at 140K [31]. The fact that He irradiation also leads to a higher loop density was also mentioned in that work but without any deep analysis of Burgers vector distribution.

Considering the strong effect of He on loop population, it is important to rationalize in which sequence He leads to the modification of the microstructural evolution, and which mechanisms may explain such a strong difference between the morphology of the loops formed in dual (He-$Fe^+$) and single ($Fe^+$) beam irradiation conditions. Sufficient understanding of the atomic-level processes that govern the mobility and growth of loops and bubbles would allow to adopt the already existing modelling tools (see e.g. [32; 33]) to predict the microstructural evolution.

The purpose of this work is to provide details of the interaction of He and He-V clusters with ½<111> and <100> dislocation loops, and quantify the mechanisms by which He may affect the mobility of dislocation loops and their mutual interaction. To do that, we perform a set of atomistic calculations using MD and MS simulations to extract He-loop interaction mechanisms and the corresponding activation energies. The simulations were carried out using two recent Fe-He potentials proposed by Juslin et al.[19] and Gao et al.[23], which are known to be essentially improved thanks to DFT data as compared to the previously exploited potential in Refs. [20; 21]. The common basis for both Fe-He potentials is the Fe-Fe embedded atom model potential developed by Ackland et al. in [34].

## 2. Computational details

MS simulations were performed in 3D and 2D periodic crystals to characterize the interaction of He with SIA clusters (including $a_0/2<111>$ and $a_0<100>$ dislocation loops) and dislocations, respectively. The relaxation was realized using a combination of conjugate gradient and quasi-dynamic relaxation techniques [35]. The relaxation was performed to reach the convergence of the force per atom of 0.1 eV/nm. To find the optimum He arrangement near a certain defect, we have attempted all possible tetra- and octahedral positions as starting points for the relaxation. The result corresponding to the lowest energy configuration is always reported. The formation energy of each particular configuration involving a combination of lattice defect(s) (SIA or vacancy) and He atom(s) embedded in the 3D-periodic bcc Fe cell is computed using the standard definition previously applied in the above mentioned works [10; 11; 12]. The He-defect interaction energy, ($E_I$), for either a substitutional or interstitial site is determined as the difference of the crystal energy when He is present near and far away from a given defect. With this notation, a negative value of $E_I$ means an attractive interaction. The binding energy ($E_b$) reported in the following is the interaction energy taken with the opposite sign. MS calculations to assess a set of binding energies for He-V and He-SIA complexes have been performed in a crystal with dimensions $20\times20\times20\times a_0^3$ (where $a_0$ is the lattice unit equal to 0.28553 nm), thus the concentration of point defects was $N_d\times6.25\times10^{-5}$ or $\sim N_d\times5\times10^{24}$ $m^{-3}$, where $N_d$ is the total number of point defects present in the system.

The MS-relaxed crystals were then used as starting configurations for MD simulations. The latter were performed within the NVE ensemble without additional temperature control, varying the MD integration time step from 0.25 to 5 fs, depending on temperature. MD simulations addressing the interaction of $He_N$-$V_M$ with SIA clusters ($I_K$ for K=1,3 and

K=7,19,37) were performed in the temperature range 100-900 K, and the evolution of the system was typically followed for 50 ns in each run. Temperature and total energy were monitored every 0.1 ns to control their conservation in each MD run. The position of the migrating defect was recorded and the diffusion coefficient, jump frequency and correlation factor was defined following the standard procedure previously used by e.g. [36; 37; 38; 39] when studying 3D and 1D migration of point defects, their clusters and interstitial impurities. Some additional computational details and formulas applied are provided in the sections describing the results.

To assist the understanding of the interaction of He with dislocation loops, we have performed additional calculations to characterize the behaviour of He near a straight dislocation line. At this, we considered both static dislocation at 0K and moving dislocation at finite temperature. The interaction of $a_0/2<111>\{110\}$ edge and $a_0/2<111>$ screw dislocations with He atoms was studied using the so called model of periodic array of dislocations developed in [35]. In this model, the $\frac{1}{2}[111](1\bar{1}0)$ edge dislocation is constructed in the crystal with principal crystallographic axes *x, y ,z* oriented along [111], $[\bar{1}\bar{1}2]$ and $[1\bar{1}0]$ directions, respectively. The *z* axis is perpendicular to the glide plane of the introduced edge dislocation. Periodic boundary conditions are imposed in the *x* and *y* directions. The boundaries in the *z* direction are formed by rigid blocks that can move along *x* and *y* to mimic external load. In the case of a screw dislocation, the dislocation line is along the *x* axis and free surfaces are applied along *y* direction. Applying a sufficiently large crystal one can ensure a negligible effect of the surface relaxation on the dislocation core structure and dislocation-He interaction, as was done in this work. In the present work, we have applied the same computational details as in our recent work in which the dislocation – loop drag was studied in the Fe-Cr system [40].

The interaction of He with a moving dislocation was studied at finite temperature applying a pure shear strain in the above described model of periodic array of dislocations. Shear is applied at constant rate so that the dislocation moves with a steady state velocity defined by the crystal geometry (i.e. dislocation density) and the deformation rate. The shear was applied by displacement of several upper atomic layers in which atoms are rigidly fixed in their positions (i.e. they do not relax in the MD loop). A crystal size and applied shear rate defined the resulting dislocation velocity, which was chosen to be 10 m/s in this study, which is a reasonable compromise between computation speed and representative crystal size large enough to avoid artifacts of the dislocation self-interaction (via imposed periodic boundaries). Note that introducing a dragging loop in the MD crystal already containing the dislocation

does not change the steady state dislocation velocity, but the resolved shear stress increases to surmount the work needed for the loop displacement. For the support of the reader, the sizes of the crystals applied, specific relaxation conditions, MD details such as integration time step and length of runs will be reported in each section separately.

## 3. Results

### 3.1. General information about He-defect interactions: benchmark of the applied potentials

Binding energies for different He-defect arrangements are presented in Tables 1 and 2. Both potentials predict a tetrahedral site as the most favourable position for an interstitial He in agreement with DFT data. As it has been mentioned in the earlier studies [22; 23], the DFT calculations demonstrate some disagreement especially for the binding energy of two interstitial He in tetrahedral sites (i.e. $He_2$ cluster). The binding energy calculated with the VASP code [10] is 0.02 eV whereas with the SIESTA [11; 13] it is 0.43 eV. The presently used potentials predict the binding energy for the $He_2$ cluster to be inside these two bounds. The formation energies for the He-rich $He_N$-$V_M$ clusters also follow well the trend obtained from the DFT.

The binding energies of $He_T$ to the core of the $a_0/2<111>$ screw and $a_0/2<111>\{110\}$ edge dislocations obtained with the potentials and DFT calculations are compared in Table 1. The profile of the interaction energy versus distance between $He_T$ and edge dislocation core is presented in Fig.1. $He_T$ is repelled in the compressed region and attracted in the tensile zone. Note that both potentials provide essentially similar curves.

$He_T$ binds stronger with the edge rather than screw dislocation, which is correctly predicted by both potentials, and the absolute values for the screw dislocation are in good agreement with the DFT result (see Table 1). The interaction range, truncated where the interaction energy goes below 0.025 eV, is about 1nm for both types of dislocations. In the case of the edge dislocation, the binding energies obtained with the potentials are underestimated by about a factor of two.

The overall evolution of the binding of $He_T$ with SIA defects is presented in Fig.2. The details of the interaction with small SIA clusters will be discussed later, while here we only mention that $He_T$-$I_K$ binding energy increases with K, i.e. with size of SIA cluster. However, even for relatively large <111> SIA clusters the binding energy still does not reach the value obtained for the edge dislocation. Hence, the interaction strength of $He_T$ with small dislocation loops, typically created in collision cascades, is in between that for screw and edge

dislocations (see Fig.2). The available DFT data for $H_T$-ED and $He_T$-SD interaction can therefore serve as reliable indicators for the actual strength of loop-$He_T$ interaction.

To provide a deeper insight to the loop-$He_T$ interaction, we have constructed linear profiles of the interaction energy for several positions in the habit plane. These curves are presented in Fig.3 and Fig.4 for $a_0/2<111>$ and $a_0<100>$ loops, respectively. Both loops contain approximately the same number of SIAs (~60 interstitials). The strongest interaction occurs at the edge of the loops, but the maximum interaction energy is significantly higher for the $a_0<100>$ loop, being 1.1 eV. Hence, $a_0<100>$ loops are expected to be the strongest microstructural features of interstitial-type trapping freely migrating He atoms.

3.2 Interaction of He-V clusters with 3D-migrating SIA clusters: Interaction mechanisms

Our earlier study, employing the potential by Juslin et.al. [19], has shown that pure He clusters of size up to four He atoms exhibit extremely fast migration in BCC Fe [41]. The mobility of the $He_N$ clusters was driven by the migration of $He_T$ detaching and getting back to the cluster. This resulted in the very low migration energy (i.e. ~0.1 eV) of the whole $He_N$ cluster, estimated directly from MD simulations by plotting the Arrhenius relationship. Practically, it was found to be comparable to the migration barrier of $He_T$ in Fe bulk (i.e. 0.07 eV). Adding more He atoms to $He_4$ cluster results in the punching of an SIA and formation of low-mobile $He_5$-$V_1$ cluster. We have checked that the potentials applied here reproduce this mechanism in accordance with the DFT results [13]. Hence, upon high energy He implantation (e.g. in [28]) one should not expect the presence of $He_N$ clusters. On the one hand, they exhibit fast migration and should attach very quickly to either an available vacancy or to dislocation defects, including dislocation loops generated in collision cascades. On the other hand, even their formation is questionable because He-induced cascades will generate numerous vacancies acting as primary source of trapping. The effective migration energy of small He-rich clusters (such as $He_{2,3,4}V_1$) was found to be ~0.3 eV [41] i.e. comparable to the migration barrier of an SIA [41]. For that reason we have studied the interaction of He-rich clusters with 3D-migrating SIA clusters applying finite temperature MD simulations.

The MD simulations were carried out in the range of 450-600K to speed up the mobility of SIA clusters placed in the same simulation box with a $He_NV_M$ cluster. In particular, we have explored the interaction of $I_K$ with $He_NV_M$ clusters, varying K=1-3 and N=M=1-4. SIA clusters with a size larger than four exhibit mixed 3D/1D or just pure 1D diffusion [42], and the interaction with such type of SIA clusters will be considered in the following section. The

observed interaction mechanisms for the 3D-migrating clusters can be subdivided depending on the outcome product as follows:

(i) Trapping without modification of the configurations of reacting clusters is the first type of the reaction mechanism. For example, that was observed for K=1:N=4:M=1; and for K=3:N=3:M=1,2 reactions. Visualization of these reactions is attached as supplementary material (see movies entitled: I1_He4V1_600K.gif and I3_He4V1_600K.gif). Generally, such reactions take place if $K \geq M$, which implies that all vacancies would recombine and either pure $He_N$ or $He_N$-$I_{K-M}$ cluster would form, which is eventually not energetically favourable. In the case of the interaction of $He_T$ with $I_K$, the dissociation was observed typically within hundreds of picoseconds at T=600K. Hence, the trapping energy is rather low (of the order of 0.2-0.3 eV taking $10^{13}$ $s^{-1}$ as attempt frequency for dissociation jumps) and is not strong enough to provide substantial immobilization of $I_K$ at room temperature. However, for the clusters containing two, three and four He atoms the binding was essential. To estimate the exact values we have performed MS calculations, presented in the following section.

(ii) The second reaction mechanism corresponds to the complete recombination of all SIAs thus converting $He_NV_M$ into $He_NV_{M-K}$ complex. Such reaction was observed only for K < M. Supplementary material contains an example of such reaction involving the interaction of $I_1$+$He_4V_2$ (see animation entitled: I1_He4V2_600K.gif). In all of the cases, such reaction mechanism indeed leads to the formation of the energetically more favourable configurations by gaining the energy due to the SIA-vacancy recombination.

### 3.3 Interaction of He-V clusters with 3D-migrating SIA clusters: Interaction energy

The interaction energy of $I_{1,2,3}$ with He-rich clusters, for which the trapping reaction was observed in MD simulations, was computed using the MS simulations. The results obtained with both applied potentials are presented in Table 3. As roughly evaluated from MD simulations, the interaction energy for $He_T$ is rather low, as it does not exceed 0.35 eV. In the case of $He_NV_1$ clusters, the binding energy is essentially higher than for $He_T$-$I_K$. The highest binding energies with the $I_K$ are found for the $He_2V$ cluster, in which the vacancy recombined with the SIA as a result of the quasi-static relaxation. For the larger He-V clusters, no recombination took place, consistently with the results of MD simulations, and the binding energy between the two clusters was found to be in the range of 0.6-1.0 eV. Note that both potentials provide consistent results with a shift of about 0.1 eV. Correspondingly, we conclude that the interaction of 3D-migrating $I_K$ with $He_NV_M$ clusters (in case when K > M) results in the strong trapping of $I_K$, for which the dissociation energy, roughly estimated as the

sum of the migration and binding energies, is above 0.9 eV. This means that such complexes would be thermally stable at room temperature for significant time (certainly much longer than the typical TEM observation timespan). Note that binding of self-interstitials in the $I_K$ cluster is practically independent of whether $I_K$ is free or attached to a $He_NV_M$ complex.

3.4 Interaction of He-V clusters with 1D-migrating SIA clusters: Interaction energy.

1D migrating SIA clusters contain five SIAs and more, thus, given the sizes of the $He_NV_M$ clusters considered here, the number of SIAs would always exceed the number of vacancies. By analogy with the 3D-migrating SIA clusters, the trapping of 1D-migrating $I_K$ is expected in the vicinity of a He-V cluster. We have computed the binding energy of $I_7$, $I_{19}$ and $I_{37}$ with $He_T$ and several $He_N$-$V_1$ clusters. The results are summarized in Table 4. One can see that the binding energy of $He_T$ increases with the cluster size K, but still does not reach the value corresponding to the interaction energy with the perfect edge dislocation (see Table 1). This is consistent with the fact that $I_{37}$ does not yet acquire the full dislocation line structure. The binding energy of 0.4-0.6 eV is not enough to stabilize the loop-$He_T$ complex at room temperature and it should breakup within a time of $\sim 10^{-3}$ seconds. So we conclude that the association of a single He atom to a small $a_0/2<111>$ dislocation loops does not produce a thermally stable configuration at room temperature. Within its lifetime, however, the loop-$He_T$ complex might, in principle, diffuse by simultaneous 1D loop glide and in-core migration of $He_T$. This migration mode, referred to as 'loop-He drag', will be explored in the following section reporting the MD results.

The interaction of $I_{7,19,37}$ with the $He_{2,3,4}$-V clusters did not reveal the annihilation of a vacancy in either considered cases. The strongest interaction was seen to occur for the $He_N$-V clusters placed in the tensile region of the cluster's edge, which was also expected, since $He_T$ exhibits the highest binding in the tensile region of the dislocation line. Note that the absolute value of the interaction energy scales with the number of He atoms, which underscores that the attraction between these two objects is provided by the He-loop and not by vacancy-loop interaction.

If one compares the variation of the interaction strength depending on the He-to-vacancy ratio for 1D and 3D migrating clusters, the trends are clearly opposite. The interaction energy of $I_{1,2,3}$ with $He_2V$ is much higher than with the $He_4V$ cluster, because the I-V recombination takes place in the former case. While, the interaction energy for $I_{7,19,37}$ raises by a factor of two as the number of He atoms forming the He-V complex increases. As mentioned above, the reason is the strong He-dislocation interaction. From that view point,

the nature of the binding with 3D and with 1D migrating clusters differs so as the absolute binding energies.

Finally, we again would like to underscore the consistency of the results obtained with the two potentials, showing the robustness of the withdrawn trends.

### 3.5 Interaction of He-V clusters with 1D-migrating SIA clusters: finite temperature simulations

The binding energies obtained for the 1D migrating SIA clusters with $He_N$-$V_1$ clusters overall exceed 1 eV, so the fast 1D migrating is expected to be totally suppressed in the presence of He-rich clusters. To confirm that, we have performed a set of MD simulations varying temperature from 100K up to 900K. Several $He_N$-$V_1$ clusters and $He_T$ were placed in the glide prism of the 1D SIA clusters at a distance of several nanometers to the habit plane to induce the interaction in the MD simulations.

The MD simulations of the interaction of $He_T$ with 1D clusters confirmed the occurrence of the He-loop drag, at least at room temperature and above it. As is shown in the supplementary animation (see movie '7SIA_1He.gif'), a fast migrating $He_T$ attaches to the edge of $I_7$ small dislocation loop and performs the migration in the tensile region of the cluster. The migration mechanism of the $He_T$ on the edge of the loop is similar to that on the core of the corresponding edge dislocation. Hence, the collective movement of a $a_0/2<111>$ loop and $He_T$ is possible thanks to the ability of $He_T$ to perform fast pipe diffusion. The analysis of the migration of $He_T$ and $He_N$ clusters on the straight line of an $a_0/2<111>\{110\}$ edge dislocation is carried in the following section.

At 100K, MD simulations involving $I_{7,19,37}$ and $He_{2,3,4}$-$V_1$ objects have shown that the SIA clusters quickly diffuse towards a He-V cluster, get trapped and remained immobile for the whole span of the MD run i.e. for 100 ns. This confirms the strong binding obtained from static simulations. At 300K and above, the MD simulations revealed that all considered $He_N$-V clusters 'dissolve' on the impinging loop, which occurs via the migration of $He_T$ from the $He_N$-V clusters to the edge of the loop and finalizes by the recombination of the vacancy with available SIAs. The resulting configuration was the dislocation loop decorated by He atoms spread on the loop's edge forming a linear cluster configuration. These configurations were then quenched down to 0K and relaxed using the MS procedure. The resulting configurations had lower potential energy that those initially obtained from MS calculations (reported in Table 4). Hence, the 'dissolution' of $He_N$-V clusters on the loops was an energetically

favourable process. Correspondingly, this type of reaction mechanism can be schematically written as $He_NV_M+I_K \rightarrow I_{K-M}He_N$.

The above presented analysis of MD simulations demonstrates that the predictions of MS calculations for 1D migrating clusters may not be appropriate because at finite temperature some reactions, apparently requiring overcoming small barriers, may lead to the effective dissolution of the He-V clusters and formation of He-decorated loops. Since our preliminary MD simulations have shown that $He_T$-$I_{7,19,37}$ actually form thermally stable 1D migrating configurations, it cannot be ruled out that multiple $He_N$-$I_K$ ($K > 7$) clusters will also form mobile complexes. To address this question we proceed with the MD simulations of the interaction of $He_N$ clusters with a straight $a_0/2<111>\{110\}$ edge dislocation, considered as a limiting case of a large $a_0/2<111>$ dislocation loop.

### 3.6 He migration in the core of a straight edge dislocation

To investigate the He-loop drag mechanism deeper we have performed several dedicated MD simulations involving a straight $a_0/2<111>\{110\}$ edge dislocation. The simulations with the edge dislocation (ED) were used to scrutinize the details of the migration mechanism of a single $He_T$ and multiple $He_N$ clusters. In the case of unloaded (and correspondingly immobile) ED, $He_T$ was seen to quickly migrate at room temperature jumping between tetrahedral positions adjacent to the core of the edge dislocation in the tensile region. The average rate of jumps in the core of the dislocation was comparable to that in BCC Fe bulk, suggesting that the in-pile migration barrier is rather low. These simulations indicate that the in-core pipe diffusion on a moving dislocation should also be possible since the $He_T$-ED binding energy, 0.8 eV, is rather high. To prove this we proceed with the MD simulations considering the ED decorated by a different number of $He_T$. External shear load is applied to induce dislocation movement at a velocity of 10 m/s.

A usual way to control the MD simulations involving dislocations is to follow shear stress – strain evolution ($\tau$-$\gamma$). Several examples for the $\tau$-$\gamma$ curves corresponding to the case of the undecorated and $He_T$-decorated ED are given in Fig.5 (see figure caption for the specific MD conditions). The undecorated ED moves with the velocity of 10 m/s, as imposed by the strain rate, and the resolved shear stress oscillates around 5-10 MPa at 100K. The Peierls stress for the considered dislocation is rather low (80 MPa) and the lattice friction is almost completely surmounted by thermal activation already at such low temperature. Once $He_T$ is added in the system, the dislocation is pinned on it, which is seen as an increase of $\tau$ up to almost 300MPa and then sudden drop takes place reflecting the unpinning from $He_T$. The

unpinned dislocation crosses the imposed periodic boundary and again interacts with $He_T$ in the same manner. This result shows that at 100K $He_T$ is not fast enough to migrate along with the ED and therefore acts as a point-defect obstacle whose strength is defined by the $He_T$-ED interaction energy profile (see Fig.1).

Raising the temperature up to 600K activates the pipe diffusion of $He_T$, and the dislocation does not unpin from $He_T$ which is fast enough to adjust its position as the ED advances. The resolved shear stress increases by ~100 MPa because of the extra force needed to drag the He atom. Adding the second $He_T$, results in a further increase of the steady-state shear stress as shown in Fig.5. Two drops seen in Fig.5 correspond to the detachment of the $He_2$ cluster from the dislocation line. However, the fast 3D migrating $He_2$ cluster almost immediately attaches back to the dislocation line, moving much slower than the $He_2$. This picture suggests that the $He_N$-ED drag may realize within a certain temperature and dislocation velocity range. The faster dislocation moves the higher temperature is required for $He_N$ to achieve sufficient in-core diffusivity. Hence, the in-core diffusivity of $He_N$ defines a lower temperature bound. The upper temperature limit is defined by the $He_N$-ED binding.

Let us now analyze in detail the pipe migration of He atoms and their unpinning from the ED in the loaded crystal. At 100K, a single $He_T$ does not migrate and the ED unpins once the critical stress of 300 MPa is achieved. Given the imposed dislocation velocity, the critical stress is reached within 0.1 ns, while the average time needed for a single He jump is ~0.33 ns assuming that the local migration barrier is 0.07 eV (i.e. the same as in bulk and attempt frequency $10^{13}$ $s^{-1}$). In practice, the migration barrier of $He_T$ in the dislocation core might be higher due to a rough relief of the interaction energy near the core (see Fig.1). This explains the absence of He drag in the simulations at 100K.

At 300K, $He_T$ exhibits limited migration along the core, and the ED frequently unpins from $He_T$. At 600K, $He_T$ intensively migrates along the dislocation line, crosses several times the periodic boundaries and does not detach during the whole MD time span i.e. 10 ns. Given that the binding energy of $He_T$-ED is 0.8 eV, the dissociation time should be about 2 μsec – much longer than the MD run. The average time required to sweep the whole dislocation line (of 5 nm length) is about 0.27 ns. By assuming that the attempt jump frequency for the in-core migration is $10^{13}$ $s^{-1}$, we estimated the activation energy for the pipe diffusion of $He_T$ to be 0.3 eV.

At 300K, $He_2$ cluster migrates towards the dislocation core and resides being immobile without appearing the pipe migration along the dislocation core. The dislocation unpins from the $He_2$ cluster once the critical stress is reached. Increasing the temperature up 600K initiates

the $He_2$ pipe migration, but the steady-state resolved shear stress for $He_2$-dislocation configuration is higher than in the case of $He_T$-ED drag. The reason why $He_2$ is stronger in the suppression of the dislocation movement can be explained by the migration mechanism. Two He interstitials cannot migrate simultaneously in the dislocation core, so they decouple and perform two consecutive jumps. This movement increases the length of the instantly pinned dislocation segment and therefore a higher shear stress is needed to displace the whole $He_2$-dislocation configuration. We expect that further growth of $He_N$ cluster leads to a stronger pinning effect.

Naturally, the suppression of the dislocation movement should also be reflected in the slowing down of $a_0/2<111>$ dislocation loops dragging He atom(s). The expected reduction of the diffusivity of $He_T$-loop complex should be proportional to the number of He atoms decorating the loop.

### 3.7 Loop-He drag

The MD simulations to study the mobility of $He_N$-$I_{7,19,37}$ complexes have been performed at 300K, 600K and 900K. Initially, the <111> SIA cluster and $He_T$ (and $He_2$, $He_3$ clusters) were placed separately at a distance of about 5 nm. Soon after thermalization, $He_N$ migrates to the edge of the 1D migrating loop and keeps diffusing in the tensile region of the dislocation line together with the loop. The decorated loop performs back and forth 1D glide.

At the highest temperature, emission of $He_T$ from the loop was frequently observed, nevertheless the diffusivity of $He_T$-loop as a single object could be measured with acceptable accuracy. At 300K, no dissociation events were detected during 50 ns.

To quantify the effect of He-decoration on the mobility of the $a_0/2<111>$ dislocation loops we have computed three main parameters defining the 1D migration process, namely: jump frequency, correlation factor and diffusion coefficient. The mathematical relation between these terms is expressed through the Einstein formula for the coefficient of diffusion of a 1D-migrating object, which is:

$$D^{d*} = f_c \frac{\nu_j \Delta^2}{2} \qquad (1)$$

Here, $\nu$ – is the cluster jump frequency, $\Delta$ – is the jump length (taken to be $|a_0/2<111>|$) and $f_c$- is the correlation factor which defines a dynamics of oscillation motion (being temperature and cluster size dependent [36]). For the 1D motion of SIA clusters, $f_c$ is defined as [36; 43]:

$$f_C = \frac{N_{forw}}{N_{back}} \qquad (2)$$

For 1D glide, $f_c$ is simply the ratio between the number of forward and backward jumps of the loop. In BCC Fe, $f_c$ is known to exceed unity for the loops of size 7-100 SIAs [36; 39; 42]. The activation energy for the diffusion and jump frequency of the small $a_0/2<111>$ interstitial loops is determined to be ~0.05 eV in the same works. The prefactor for the jump frequency decreases as $N^{-S}$, where $N$ is the number of SIAs and S~0.64 for Fe [36], so the larger the loop the smaller the prefactor.

The diffusion characteristics and activation parameters, extracted using the Arrhenius relationship, are presented in Fig 6. As one sees, the decoration by $He_N$ progressively reduces the correlation factor, which becomes one half at room temperature for the $He_3$-loop complex, see Fig.6(a). Physically, the reduction of $f_c$ implies that the decorated loop exhibits a higher probability for correlated backward jump, which overall results in the decrease of the absolute diffusion coefficient. Beside that, the activation energy for the jump frequency also increases from 0.07 eV up to 0.14 eV for the $He_3$ decorating the loop, Fig.6(b). The cumulative effect results in the reduction of the diffusion coefficient by one order of magnitude at room temperature for the loop migrating with two or three He atoms attached, see Fig.6(c). Since, both activation energy for the loop jump and the correlation factor change monotonically with a number of decorating He atoms, we conclude that the pipe migration of $He_T$ in the tensile edge of the loop controls the mobility of the whole complex. It is reasonable to assume that with the increase of the number of decorating He atoms (tending to form a cluster in the edge of the loop), the loop will be completely immobilized and its dissociation will be controlled by the $He_N$-$I_K$ binding energy function.

## 4. Discussion, conclusions and outlook

In this report, we have performed a critical review of the available results of atomistic simulations regarding the interaction of He with point- and extended defects in BCC Fe. The analysis of the available data, in the light of recent experimental study of Prokhodtseva et al.[28] reporting a strong effect of He on dislocation loop population, evidences an incomplete understanding of the interaction of He and $He_N$-$V_M$ complexes with SIA defects, namely with small 3D- and medium/large 1D-migrating clusters. This work is the first step, where we systematically address this problem using two recent DFT-fitted empirical potentials for the Fe-He system.

Both potentials provide a reasonable agreement with DFT considering the formation energy of small He-V clusters, stability of $He_T$ and $He_T$-$He_T$ interaction in the BCC Fe bulk. Both potentials provide similar qualitative and quantitative description of the interaction of $He_T$ and He-V clusters with 3D- and 1D–migrating SIA clusters and straight dislocations. Therefore, large scale MD simulations were performed employing only one of the tested potentials, developed by Juslin et al.[19]. The analysis of the obtained MD results allows to put forward two principal statements:

1. $He_T$ exhibits weak attractive interaction with a single SIA, but the binding energy raises for larger clusters, which gradually transform to dislocation loops. He-V complexes exhibit attractive interaction with both 3D and 1D migrating SIA clusters, however, the nature of the binding is different. The attractive interaction for the 3D clusters is driven by the vacancy-SIA recombination. While the attractive interaction with the 1D-migrating SIA clusters and dislocation loops originates from the binding of He to the tensile dislocation zone.

2. MD simulations revealed a combined movement of $a_0/2<111>$ loop being decorated by $He_T$ and $He_N$ clusters. This movement can be classified as $He_N$-loop drag and up to our knowledge, this effect for He in bcc Fe is reported for the first time here. A detailed analysis performed for a seven SIA cluster showed that $He_N$-decoration causes strong reduction of loop diffusivity (10 times at room temperature) related to the enhancement of the correlated motion and raise of the activation energy for migration. Based on the dependence of the diffusion parameters on the number of decorating He atoms, it is concluded that mobility of the decorated loop is controlled by the pipe migration of He in the edge of the loop. Eventually, a decorated $a_0/2<111>$ dislocation loop can be completely immobilized given that the number of decorating $He_T$ atoms will reach a critical value. From that moment on, the movement of the loop will be initiated only after the dissociation from $He_N$ cluster.

Given the provided above analysis of the MD and MS results it is possible to reason and propose a scenario for the explanation of the experimental observations of Prokhodseva et al.[28], namely: the strong suppression of the density of $a_0<100>$ loops observed after dual implantation at room temperature in ultra high pure Fe. In particular, depending on surface orientation, the fraction of the ex-situ observed $a_0<100>$ loops varied from 0 to ~16%. While in the single beam irradiation, it was 56-100%.

As was already discussed by Prokhodseva et al.[28], the experimental observations suggest that <100> loops originate from the interaction between in-cascade created $a_0/2<111>$ loops, so their low fraction in the single beam irradiation is explained by two competing phenomena: mutual interaction producing <100> loops and disappearance at the foil surface.

In the dual beam irradiation, non-recombined SIAs contribute to the growth of SIA clusters and loops, while He ions associate with vacancy(ies) forming He-$V_N$ clusters. The latter exhibit much lower diffusivity as compared to $a_0/2<111>$ loops, and represent 'barriers' suppressing 1D migration of the dislocation loops. As a result of the interaction of $I_K$ with He-$V_N$, He atom is accommodated in the loop's edge, vacancies recombine and He-$I_{K-N}$ complex continues to glide. If the dose rate is sufficiently high, He-$I_{K-N}$ complex will survive till another He-V complex will appear in its glide prism. The second He atom will also be absorbed on the loop's edge, resulting in the further reduction of the loop diffusivity. This process goes on until a sufficient number of He atoms will decorate the loop to reduce its mobility so strongly that a newly created 3D migrating SIA defects will be faster and therefore will contribute to the loop growth. This way, He-decoration on in-cascade created $a_0/2<111>$ loops may prevent their disappearance at free surfaces and ensure their growth as well as immobilization.

Under dual beam exposure, the rate of the interactions between in-cascade created (i.e. similar in size) $a_0/2<111>$ loops will also be reduced because of the intensive interaction with He-$V_N$ clusters. Indeed, the system will contain two types of loops: just created ones (of size 0.5-1nm i.e. 7-37 SIAs) and survived from the previous cascades and stabilized by He decoration. This should correspondingly result in the reduction of the formation of <100> loops, as observed experimentally.

The quantitative validation of the presented above scenario requires rather complex and detailed OKMC simulations where the He-Loop and Loop-Loop interactions can be parameterized as close as possible to that seen in the presented MD simulations. However, the high rates of migration of 1D migrating objects, such as dislocation loops, strongly limit the timestep to small values in OKMC simulations, which thus require an extensive computational effort. This limitation is inherent to the residence-time algorithm [44] upon which OKMC models are based and according to which the timestep is inversely proportional to the total event rate. In addition, loops generally appear in low densities, which can lead to a problem of statistical representation due to the relatively small simulation volume reachable by OKMC models. To circumvent these problems, the scenario proposed in this work can also be simulated using a Rate Theory approach, which is not limited by event rates nor by object density. In Appendix 1, we provide an outlook for the application of Rate Theory approach, which will be used in the follow up of this work.

Besides, the problem of the up-scaling of the already obtained results, there is still some missing information important to complete the picture. As an outlook, we see the following issues to be addressed:

1. Extend the simulations to study He-loop drag, its dependence on a number of He atoms, elucidate the mechanism of SIA punching and formation of stable $He_N$-$V_M$ cluster on the edge of SIA loops. Determine at which conditions the mobility of He-Loop complexes becomes comparable to 3D SIA clusters and to vacancy migration. These data will provide knowledge about prevailing types of reaction rates expected to play the main role in the process of the microstructural evolution on the time scale typical for cascade annealing (i.e. ~μs).
2. Reconsider the interaction between two $a_0/2<111>$ SIA loops being decorated by He atoms and see how the He decoration affects their interaction and formation of <100> loops.
3. Re-assess the validity and accuracy of available Fe-He potentials focusing on the properties of He in the core of dislocations and grain boundaries, as the latter represent useful examples of highly disturbed lattice regions but manageable at DFT space scale.
4. Identify the size of He-V clusters which behaves as a bubble and therefore will not follow the atomic-type reactions resulting in vacancy recombination as considered in the present report. This information is another crucial input for upper scale models i.e. RT or OKMC.

Acknowledgements:
The Spanish Secretariat of Research, Development and Innovation (FIS2012-39443-C02-02) .
The work was partially supported by the EUROfusion programme.

Appendix 1. Outlook for rate theory application.

In the Rate Theory framework, the diffusion of mobile species is governed by a set of coupled diffusion-reaction equations, whereas the nucleation and/or growth of clusters is described by the so-called Master equation (see e.g. [45; 46]). Similarly to what is done in OKMC models, in the RT approach reactions are assumed to occur via bimolecular interaction. The formalism therefore requires the reaction constants and the reaction rates as input, which can be calculated as done in Ref. [45], for instance. According to the scenario of microstructural evolution described in Section 4, the main species that form under He irradiation or dual beam are $HeV_N$ clusters, I, V, $V_N$ and $I_K$ clusters. The basic binary reactions necessary to describe the evolution of He, vacancies and self-interstitial species in Fe under the discussed irradiation conditions are:

$$I_K + V \rightarrow I_{K-1} \quad (3.1)$$

$$I_K + I_M \rightarrow I_{K+M} \quad (3.2)$$

$$V_M + V \rightarrow V_{M+1} \quad (3.3)$$

$$V_M + I_K \rightarrow V_{M-K} / I_{K-M} \quad (3.4)$$

$$HeV_M + I_K \rightarrow HeV_{M-K} / HeI_{K-M} \quad (3.5)$$

As mentioned above, $HeI_K$ complexes are expected to be mobile (at least at room temperature) so their glide and interaction with other defects should lead to the formation of new species not formed directly in cascades:

$$HeI_M + HeI_K \rightarrow He_2I_{M+K} \quad (4.1)$$

$$V_M + HeI_K \rightarrow HeI_{K-M} / HeV_{M-K} \quad (4.2)$$

$$HeV_M + HeI_K \rightarrow He_2I_{K-M} / He_2V_{M-K} \quad (4.3)$$

$$HeI_M + I_K \rightarrow HeI_{M+K} \quad (4.4)$$

In the reactions defined above, we assumed that a self-interstitial cannot dissociate from $I_K$ or $He_NI_K$ complexes due to their relatively high binding energy (exceeding 2 eV [47]). We also assumed that $He_NI_K$ clusters with $N \geq 2$ are immobile since their diffusivity is strongly reduced as the number of He atoms decorating the loop increases, which was shown above by direct MD simulations. Then, following the Rate Theory formalism and the atomistic mechanisms proposed above, we obtain the set of Partial Differential Equations (PDEs) governing the evolution of the concentration of the different species in the system. For instance, for the concentration of self-interstitials, we obtain:

(5)

$$\frac{\partial C_I}{\partial t} = D_I \nabla^2 C_I + GR_{I_2+V} + GR_{I_K+I} + GR_{V_M+I} + GR_{HeV_M+I} + GR_{HeI_M+I}$$

The first term on the Right Hand Side (RHS) in equation (5) represents the diffusion term due to the gradient of concentration. $GR_X$ terms appearing in the RHS stand for the generation-recombination (GR) terms due to the different reactions in which the defect is involved. Specifically, in the case of self-interstitials, the second term of the RHS results from the creation of self-interstitials by annihilation of $I_2$ clusters and vacancies. The third term of the RHS corresponds to the agglomeration of self-interstitials into clusters $I_K$. Next term accounts for the recombination of self-interstitials with vacancy clusters. Fifth GR term takes into account the annihilation of self-interstitials at vacancy clusters but containing one He atom. Finally, last term results from the growth of $HeI_M$ clusters by attachment of self-interstitials. The expression of the different $GR_X$ terms can be easily derived, as it is done in [45].

In a similar way, the evolution equations can be derived for the rest of the species, taking into account their mobility and the different reactions in which they are involved. However, one has to know that in some cases, deriving an exact expression for rates of reactions becomes difficult, as it is the case for the reaction between two 1D migrating objects. In this case, OKMC simulations could serve to provide effective representation of interactions and deliver necessary reaction rates to be used in the RT model.

## 5. References:


[1]M. Samaras, Materials Today 12 (2009) 46.
[2]K. Arakawa, R. Imamura, K. Ohota, K. Ono, Journal of Applied Physics 89 (2001) 4752.
[3]K. Ono, K. Arakawa, K. Hojou, Journal of Nuclear Materials 307-311 (2002) 1507.
[4]P. Dauben, R. Wahi, H. Wollenberger, Journal of Nuclear Materials 133-134 (1985) 619.
[5]P. Dauben, R. Wahi, H. Wollenberger, Journal of Nuclear Materials 141-143 (1986) 723.
[6]H. Benfu, H. Kinoshita, H. Takahashi, Journal of Nuclear Materials 258-263 (1998) 1708.
[7]H. Benfu, H. Kinoshita, T. Shibayama, H. Takahashi, Materials Transactions 43 (2002) 622.
[8]F. Garner, D. Gelles, L. Greenwood, T. Okita, N. Sekimura, W. Wolfer, Journal of Nuclear Materials 329-333 (2004) 1008.
[9]K. Arakawa, H. Mori, K. Ono, Journal of Nuclear Materials 307-311 (2002) 272.
[10]T. Seletskaia, Y. Osetsky, R.E. Stoller, G.M. Stocks, Physical Review Letters 94 (2005) 046403.
[11]C. Fu, F. Willaime, Physical Review B 72 (2005) 064117.
[12]L. Ventelon, B.D. Wirth, C. Domain, Journal of Nuclear Materials 351 (2006) 119.
[13]C.C. Fu, F. Willaime, Journal of Nuclear Materials 367 (2007) 244.
[14]G. Ackland, D. Bacon, A. Calder, T. Harry, Philosophical Magazine A 75 (1997) 713.
[15]W.D. Wilson, R.D. Johnson, Interatomic potential and simulation of lattice defects, Plenum, 1972, pp. 375.

[16]W.D. Wilson, M.I. Baskes, C.L. Bisson, Physical Review B 13 (1976) 2470.
[17]W.D. Wilson, C.L. Bisson, M.I. Baskes, Physical Review B 24 (1981) 5616.
[18]L. Malerba, et al., Journal of Nuclear Materials 406 (2010) 19.
[19]N. Juslin, K. Nordlund, Journal of Nuclear Materials 382 (2008) 143.
[20]H.L. Heinisch, F. Gao, R.J. Kurtz, E.A. Le, Journal of Nuclear Materials 351 (2006) 141.
[21]H.L. Heinisch, F. Gao, R.J. Kurtz, Journal of Nuclear Materials 367-370 (2007) 311.
[22]N. Gao, M. Samaras, E. Van Swygenhoven, Journal of Nuclear Materials 400 (2010) 240.
[23]F. Gao, H.Q. Deng, H.L. Heinisch, R.J. Kurtz, Journal of Nuclear Materials 418 (2011) 115.
[24]P.H. Chen, X.C. Lai, K.Z. Liu, X.L. Wang, B. Bai, B.Y. Ao, Y. Long, Journal of Nuclear Materials 405 (2010) 156.
[25]D.M. Stewart, Y.N. Osetsky, R.E. Stoller, S.I. Golubov, T. Seletskaia, P.J. Kamenski, Philosophical Magazine 90 (2010) 935.
[26]L. Yang, X.T. Zu, Z.G. Wang, F. Gao, X.Y. Wang, H.L. Heinisch, R.J. Kurtz, Nuclear Instruments and Methods in Physics Research B 265 (2007) 541.
[27]Y. Wang, Q. Xu, T. Yoshiie, Z. Pan, Journal of Nuclear Materials 376 (2008) 133.
[28]A. Prokhodtseva, B. Decamps, A. Ramar, R. Schaublin, Acta Materialia 61 (2013) 6958.
[29]D. Brimbal, B. Decamps, A. Barbu, E. Meslin, J. Henry, Journal of Nuclear Materials 418 (2011) 313.
[30]D. Brimbal, E. Meslin, J. Henry, B. Decamps, A. Barbu, Acta Materialia 61 (2013) 4757.
[31]K. Arakawa, H. Mori, K. Ono, Journal of Nuclear Materials 307-311 (2002) 272.
[32]C.J. Ortiz, M.J. Caturla, C.C. Fu, F. Willaime, Physical Review B 75 (2007) 100102.
[33]M. Caturla, C. Ortiz, C. Fu, Comptes Rendus Physique 9 (2008) 401.
[34]G. Ackland, M. Mendelev, D. Srolovitz, S. Han, A. Barashev, Journal of Physics: Condensed Matter 16 (2004) 1.
[35]Y.N. Osetsky, D.J. Bacon, Modelling and Simulation in Materials Science and Engineering 11 (2003) 427.
[36]Y. Osetsky, D. Bacon, A. Serra, B. Singh, S. Golubov, Philosophical Magazine 83 (2003) 61.
[37]J. Marian, B. Wirth, A. Caro, B. Sadigh, G. Odette, J. Perlado, T. Diaz de la Rubia, Physical Review B 65 (2002) 144102.
[38]K. Tapasa, A. Barashev, D. Bacon, Y. Osetsky, Acta Materialia 55 (2007) 1.
[39]N. Anento, A. Serra, Y.N. Osetsky, Model. Simul. Mater. Sci. Engrg 18 (2010) 025008.
[40]D. Terentyev, A. Bakaev, Journal of Physics-Condensed Matter 25 (2013) 265702.
[41]D. Terentyev, N. Juslin, K. Nordlund, N. Sandberg, Journal of Applied Physics 105 (2009) 103509.
[42]D. Terentyev, L. Malerba, M. Hou, Physical Review B 74 (2007) 104108.
[43]A.V. Barashev, Y.N. Osetsky, D.J. Bacon, Philosophical Magazine A 80 (2000) 2709.
[44]A.B. Bortz, M.H. Kalos, J.L. Lebowitz, Journal of Computational Physics 17 (1975) 10.
[45]C. Ortiz, M. Caturla, Physical Review B 75 (2007) 184101.
[46]S. Golubov, B. Singh, H. Trinkaus, Journal of Nuclear Materials 276 (2000) 78.
[47]D. Terentyev, L. Malerba, Journal of Nuclear Materials 377 (2008) 141.
[48]T. Seletskaia, Y. Osetsky, R. Stoller, G. Stocks, Journal of Nuclear Materials 351 (2006) 109.
[49]Y. Zhao, G.-H. Lu, Modelling Simul. Mater. Sci. Eng 19 (2011) 065004.

Tables:

Table 1. Comparison of the basic set of formation and interaction energies as obtained by the applied here interatomic potentials and available DFT data. Formation energy of a He atom in

a tetrahedral/octahedral position, $E_{T/O}$. Interaction energy between two He atoms placed in tetrahedral sites at the *N*th nearest neighbour distance, $E_I$(T-T *N*nn). Interaction energy between He atom placed in a tetrahedral site and ½<111> screw/edge dislocation*, $E_b$(T-SD/ED). To compute the above mentioned set of the formation and interaction energies the following set of formation energies for point defects was used: vacancy formation energy = 1.72 eV; SIA formation energy= 3.54 eV; Cohesive energy =-4.013 eV.

| | $E_O$ | $E_T$ | $E_I$(T-T 1nn) | $E_I$(T-T 2nn) | $E_I$(T-SD) | $E_I$(T-ED) |
|---|---|---|---|---|---|---|
| Juslin | 4.51 | 4.39 | 0.13 | 0.08 | 0.3 | 0.8 |
| Gao | 4.47 | 4.38 | 0.15 | 0.16 | 0.45 | 0.92 |
| DFT | 4.57a<br>4.60b | 4.39a<br>4.37b | 0.43a<br>0.02b | | 0.49c | 1.66c |

* edge dislocation with a {110} glide plane.
a: Fu [11; 13], b: Seletskaya [10; 48]; c: Zhao [49].

Table 2. Formation energy of the He-vacancy clusters (eV).

| | $E_{sub}$ | $He_2$-V | $He_3$-V | $He_T$-$He_T$ | He-V2 | He-V3 | He-V4 |
|---|---|---|---|---|---|---|---|
| Juslin | 4.10 | 7.43 | 10.68 | 8.65 | 5.39 | 6.33 | 6.98 |
| Gao | 3.76 | 6.90 | 9.98 | 8.49 | 4.96 | 5.89 | 6.51 |
| DFT | 4.22a<br>4.08b | 6.63b | 9.94b | 8.72 | 5.5 | 6.6 | 7.55 |

Table 3. Binding energy (eV) of 3D migrating SIA defects with $He_T$ and a number of the He-rich cluster. 'R' stands for the case when the vacancy was recombined with the SIA in the fully relaxed configuration at 0K.

| Juslin potential | He – tetra | He2V | He3V | He4V |
|---|---|---|---|---|
| I1 | 0.15 | 2.1 R | 1.5 R | 0.65 |
| I2 | 0.20 | 1.75 R | 0.8 | 0.8 |
| I3 | 0.27 | 1.75 R | 1.0 | 1.0 |

| Gao potential | He – tetra | He2V | He3V | He4V |
|---|---|---|---|---|
| I1 | 0.20 | 1.8 R | 1.1 R | 0.9 |
| I2 | 0.27 | 1.4 R | 0.6 | 0.9 |
| I3 | 0.34 | 1.4 R | 0.6 | 0.8 |

Table 4. Binding energy (eV) of 1D migrating SIA defects with $He_T$ and a number of the He-rich cluster.

| Juslin potential | He – tetra | He2V | He3V | He4V |
|---|---|---|---|---|
| I7 | 0.48 | 1.25 | 1.0 | 1.5 |
| I19 | 0.49 | 1.25 | 1.0 | 1.8 |
| I37 | 0.5 | 1.25 | 1.25 | 1.8 |

| Gao potential | He – tetra | He2V | He3V | He4V |
|---|---|---|---|---|
| I7 | 0.4 | 1.0 | 1.0 | 1.6 |
| I19 | 0.42 | 0.75 | 1.0 | 1.75 |
| I37 | 0.6 | 1.0 | 1.25 | 2.0 |

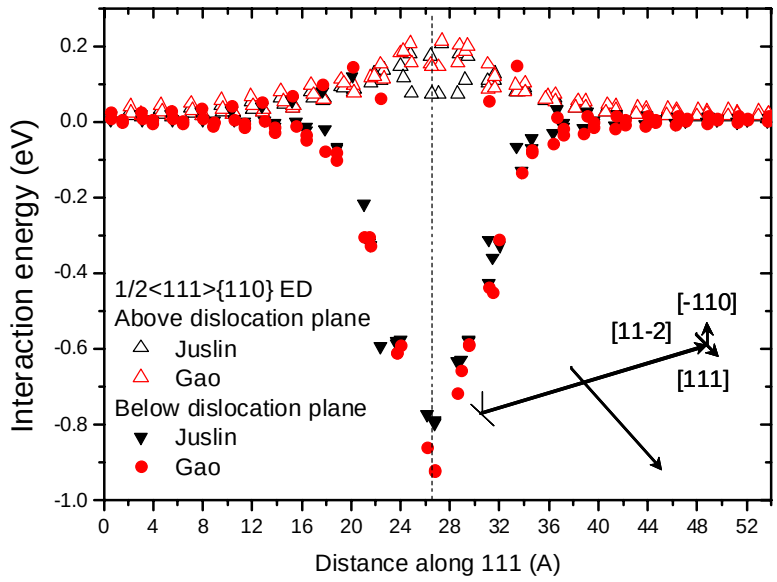


Fig.1 Interaction energy of $He_T$ versus distance from the dislocation core. The schematics for the interaction geometry is shown on the inset figure.

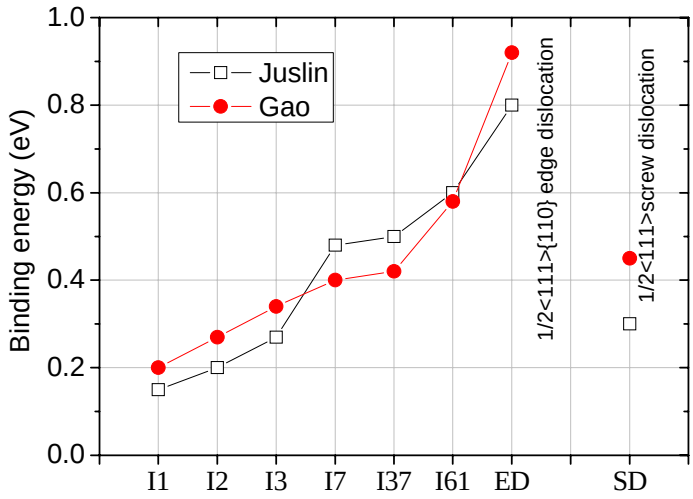


Fig.2. Binding energy of $He_T$ to SIA clusters of different size and two types of dislocations. Here, SIA cluster of size 7, 37 and 61 SIA consist of <111> crowdions i.e. are small $a_0/2$<111> dislocation loops.

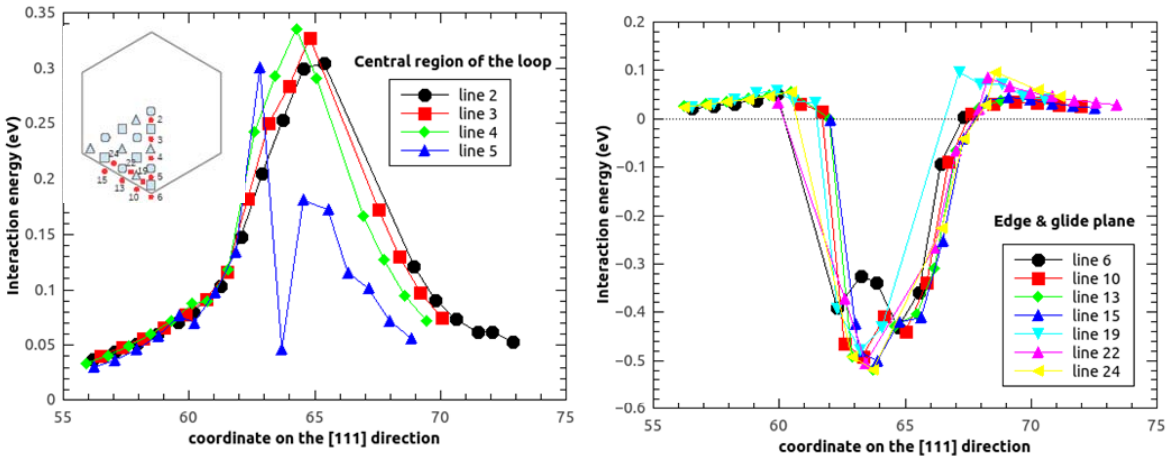


Fig.3. Linear interaction energy profile for $a_0/2<111>$ loop containing 61 SIAs. The energy profiles are obtained for several lines normal to the loop habit plane as shown schematically and enumerated on the inset left-hand side figure.

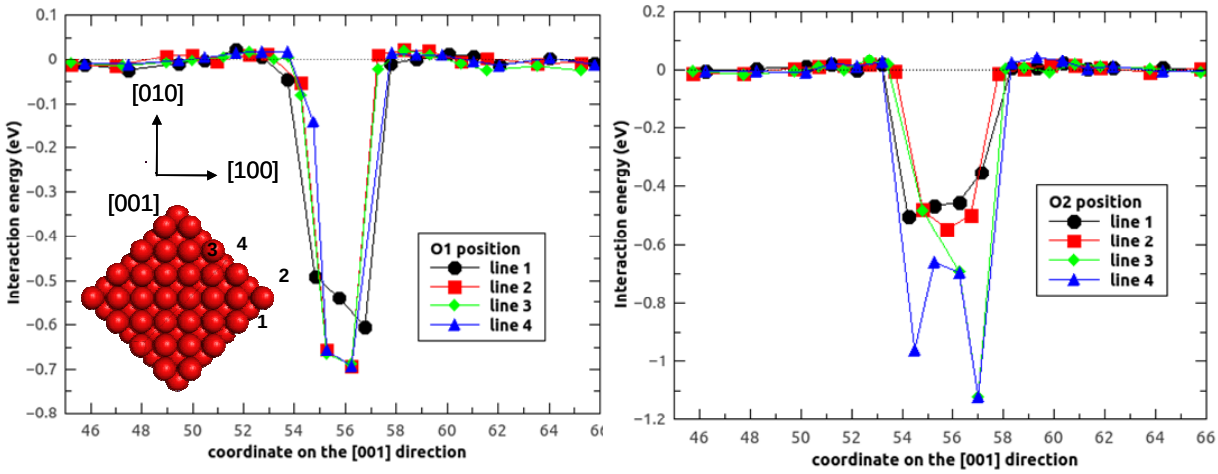


Fig.4. Linear interaction energy profile for $a_0<001>$ loop containing 64 SIAs. The energy profiles are obtained for several lines normal to the loop habit plane as shown schematically and enumerated on the inset left-hand side figure.

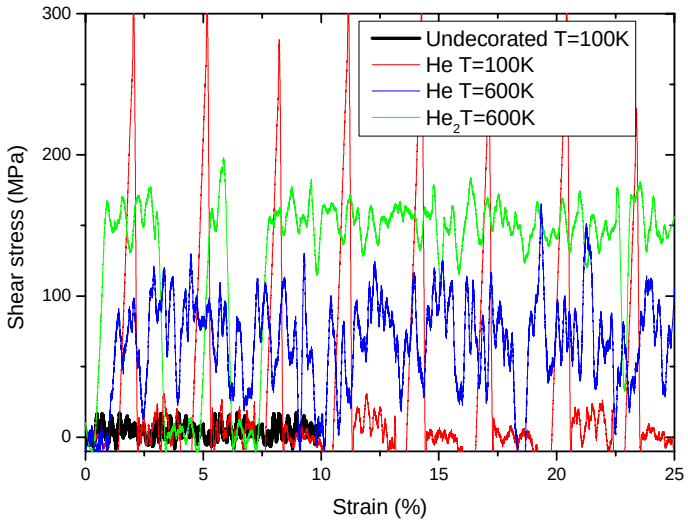


Fig.5 Stress-strain relationship for the $a_0/2<111>\{110\}$ edge dislocation loaded at 100, 300 and 600K being undecorated and decorated by one or two $He_T$ atoms. The crystallite contains 50 thousands atoms and has size 39 – 5 – 39 elementary replicas along x-y-z directions, the resulting dislocation velocity is 10 m/s.

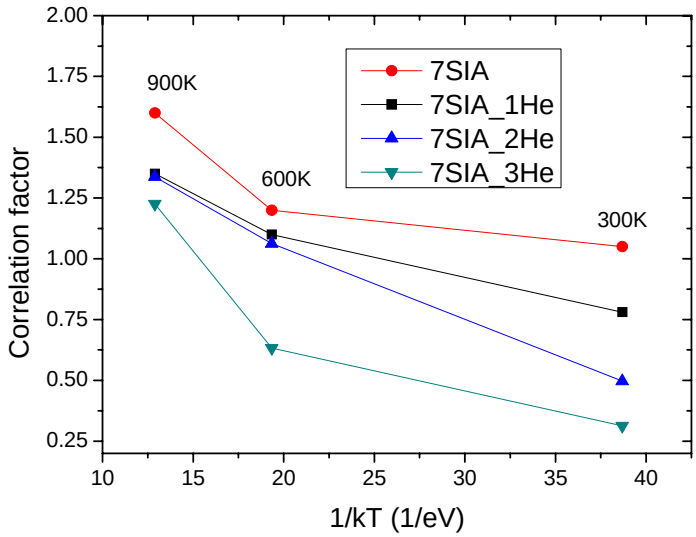
Correlation factor
1/kT (1/eV)
900K
600K
300K
7SIA
7SIA_1He
7SIA_2He
7SIA_3He

(a)

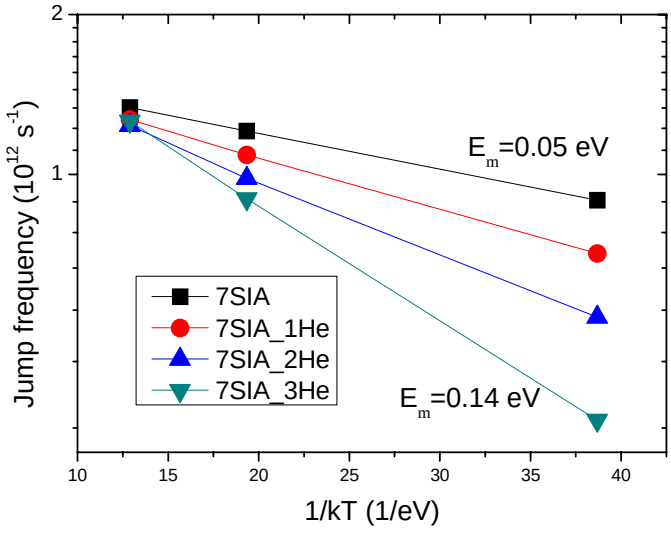
Jump frequency (10^12 s^-1)
1/kT (1/eV)
E_m=0.05 eV
E_m=0.14 eV
7SIA
7SIA_1He
7SIA_2He
7SIA_3He

(b)

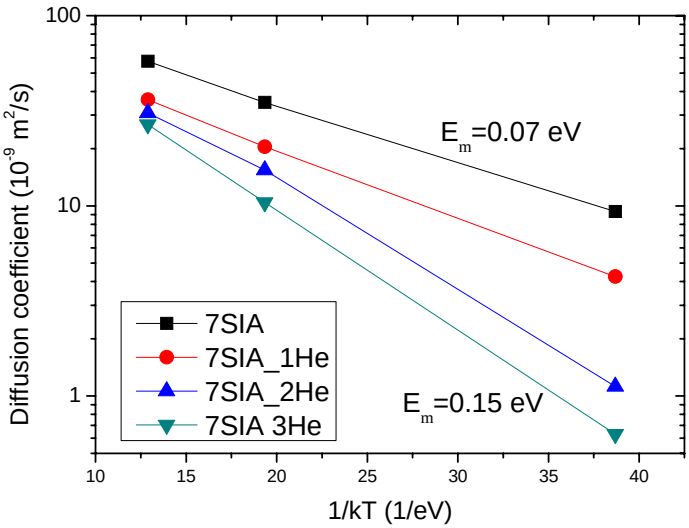


(c)

Fig 6. (a) Correlation factor, (b) Jump frequency along <111> direction and (c) 1D diffusion coefficient for the 7 SIA cluster, being undecorated and decorated by $He_T$, $He_2$ and $He_3$ clusters.